**Journal of Mathematical Modeling and Fractional Calculus**
https://acspublisher.com/journals/index.php/jmmfc
**Received:**16-05-2026, **Revised:** 14-06-2026,
**Accepted:** 18-06-2024, **Published:** 20-06-2026,
https://doi.org/10.48165/jmmfc.2026.3107,3(1),1-20 3(1),122-147.

# Chaos, bifurcation and statistical analysis of rubella disease dynamical system by utilizing different fractional approach

Usama Atta[a*]

[a]Department of Mathematics, Ghazi University, D.G. Khan 32200, Pakistan
Corresponding author Email:usamaatta1111@gmail.com

**Abstract:** Rubella is a virus cause serious health problems, particularly for expectant mothers and their unborn children. Understanding its dynamical transitions is crucial for elimination strategies. In this paper, we suggest SVEIR model Rubella model that captures the lifelong immunity after natural infection acquired through vaccination. This work presents the dynamics of Rubella spread using fractal fractional Mittag Leffler operator and Atangana Baleanu Caputo operator. Both of the operators provide reliable solutions in simulation, while the fractal fractional derivative provide better results then ABC operator due to its fractal structure solved through Newton polynomial based numerical approach. A comprehensive mathematical examination of the suggested model is presented, covering existence of bounded and positive solution, convergence and stability. We also prove the existence of transcritical bifurcation at $R_0 = 1$ using center manifold theory, which determines the threshold between disease elimination and endemic persistence. We provide impact of parameters through 3D bar plot that shows transmission rate and vaccination rate are very important in Rubella disease dynamics. The chaos test shows that model experiences bounded behaviour and does not exhibit chaotic oscillations. The statistical analysis provides information about symmetric behaviour of the compartments of the model. The work serves as a complete reference for mathematical modeling of rubella control.
**Keywords:** Rubella, Chaos test, Lyapunov function, Transcritical bifurcation, Fractional derivative, Fractal-fractional operator, Mittag Leffler Kernel, Statistical analysis.

## 1. Introduction

### *1.1. Background of Rubella disease*

Rubella (German measles) is a contagious viral infection causing a mild rash, fever, and swollen lymph nodes. While usually mild in children, it is extremely dangerous during pregnancy, especially in the first trimester, as it can cause congenital rubella syndrome (CRS) leading to miscarriage, stillbirth, or severe birth defects including hearing loss, cataracts, and heart disease. The virus spreads through respiratory droplets, coughing, sneezing, and contaminated surfaces. There is no specific treatment; symptoms resolve on their own with supportive care. The MMR vaccine is highly effective and the best prevention. Rubella was declared eliminated in the US in 2004, but cases still occur due to international travel and declining vaccination rates. Maintaining over 95% vaccination coverage is essential to prevent outbreaks and protect pregnant women [1, 2].

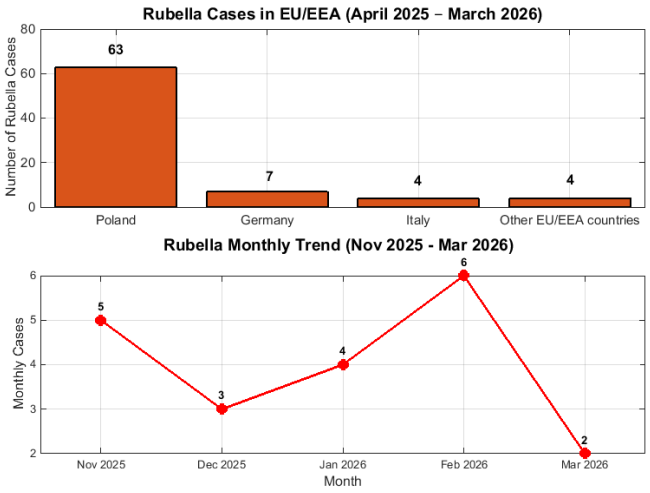


**Figure 1:** Plot showing cases of Rubella from April 2025 to March 2026

### *1.2. Literature review*

Mathematical models play a crucial role in understanding rubella transmission dynamics, predicting outbreak patterns, and evaluating control strategies. Here we are providing the short summary of the recent studies on Rubella modeling utilizing integer-order operator in Table 1.

Traditional integer-order differential equations assume that the rate of change of a population depends only on the current state. However, biological and epidemiological processes exhibit memory effects and non-local interactions that cannot be captured by classical derivatives. The following factors motivate the use of fractional and fractal-fractional operators for rubella modeling: Rubella infection induces lifelong immunity after recovery. However, the waning of vaccine-induced immunity is not instantaneous but follows a power-law decay pattern. Fractional derivatives naturally incorporate this long-term memory, making them ideal for modeling by studying duration of vaccine protection, by capturing duration of maternal antibodies in newborns, capturing long-term immune response after natural infection. Rubella transmission involves complex social contact patterns that are inherently non-local in time. An individual's infection risk depends not only on current infectious individuals but also on past exposure history. The Mittag-Leffler kernel in ABC and FFM operators captures this non-local behavior. The fractal-fractional approach accounts for the fractal nature of contact networks. Rubella spreads through household contacts, school/ workplace contacts, community transmission. The fractal dimension captures this multi-scale mixing pattern. Studies have shown that disease spread in heterogeneous populations follows anomalous diffusion rather than classical diffusion. The fractal-fractional operator naturally handles such behavior. Epidemiological data often exhibit heavy tails and long-range correlations. Fractional models provide better fit to real rubella incidence data compared to integer-order models, especially for outbreak duration distributions, inter-outbreak intervals, spatial spread patterns.

Till now, many fractional derivatives have been defined, such as conformable derivative [16, 17], Caputo Fabrizio based on singular kernel [18, 19] and Atangana Baleanu derivative based on non-local and non-singular kernel [20]. In 2017, [21] introduced fractal fractional derivative which has been widely used by researchers due to combination of fractional and fractal operators. In this study, we use both ABC and fractal fractional derivative with Mittag Leffler kernel to study Rubella disease spread.

The short summary of the recent studies on Rubella modeling utilizing fractional-order operators is provided in Table 2.

### *1.3. Contributions of the study*

The main contributions of this study are as follows: We suggest Rubella SVEIR model incorporating lifelong immunity after infection, vaccination, latent period before infectiousness. We also present a complete mathematical analysis including presence of a positive bounded solution, stability of equilibrium points, the basic reproduction number $R_0$, verification of the occurrence of transcritical bifurcation at $R_0 = 1$, impact of parameters through 3D bar, statistical analysis of all compartments and verification of bounded behaviour through chaos 0-1 test. We provide the comparison of ABC and FFM operators with different fractional orders at various dimensions solved through Newton polynomial based scheme.

**Table 1:** Summary of key contributions and outcomes from recent Rubella models.

| Sr. No. | Main Contributions | Outcomes | Citation |
|---|---|---|---|
| 1 | SEIR model with effect of vaccination. | comparison of R-K Four and R-K 45 revealed that R-K 45 performs better than RK4 in terms of the accuracy. | [3] |
| 2 | Studied co-circulation dynamics of measles and rubella incorporating eleven compartments, studied waning of partial vaccine-induced immunity, early detection and isolation, vaccination rate, and vertical transmission of rubella. | Increasing early detection and implementing dynamic vaccination reduce disease prevalence and resurgence risk, whereas waning of partial immunity can lead to resurgence. | [4] |
| 3 | Rubella model with double-dose vaccination strategy, used Euler, Rk-4 and NSFD method. Convergence and consistency analysis of NSFD scheme were proven. | NSFD is more reliable than Euler and RK4. Incorporating NSFD enhanced the model's accuracy and stability. | [5] |
| 4 | Periodic SVPEAIRS model with real data to examine the impact of vaccination, analyzed bifurcation. | Rubella cases in China fluctuate with seasonal changes, declining vaccination rate or the recovery rate rises Rubella epidemic. Increased social activities facilitate viral transmission. | [6] |
| 5 | Deterministic and stochastic model, considering vertical transmission and environmental factors with susceptible, first vaccinated, protected, infected, and recovered compartments. | Stochastic reproductive number is smaller than the deterministic. Reducing vertical infection and transmission rates and increasing vaccination and recovery rates can control the spread of rubella. | [7] |
| 6 | Rubella model including vaccination rate, vaccine waning rate, recovery rate, and progression rate from infection to severe cases with actual data. | Sensitivity analysis using the PRCC approach, achieving at least 70 % vaccination coverage minimizes cumulative new rubella cases, vaccine waning increases the disease burden. | [8] |
| 7 | Measles and Rubella model incorporating vaccination with 9 classes, computed disease-free equilibrium point, the measles-free equilibrium point, the Rubella-free equilibrium point, and the endemic equilibrium point, Two reproduction numbers, corresponding to spread of measles and rubella. | Increasing the early-vaccination and full-vaccination process reduce the measles and rubella infection. | [9] |
| 8 | SIR Rubella model . | Rubella vaccine can control infection. Vertical transmission results in increasing the number of infected persons, the interaction between susceptible and infected increases the number of infected people, while treatment can control infection. | [10] |
| 9 | Susceptible, vaccinated, protected, exposed, infected, recovered model. | Increasing contact rate, vertical transmission rate, exposure rate and rate of vaccination waning rise Rubella spread. Increasing the vaccination rate and treatment rate can help to control rubella. The number of infections increases with the birth of infected children due to infection of mother. | [11] |
| 10 | SEITR optimal control model utilizing vaccination and treatment as preventive measures to reduce the number of individuals infected within the human population and the cost of controls, NSFD, bifurcation. | Combination of all controls yields the maximum output. | [12] |
| 11 | Rubella optimal control model with vertical transmission incorporating vaccination and treatment, unique endemic equilibrium confirms the global stability and the absence of backward bifurcation. | Isolation and treatment reduces infected humans. | [13] |
| 12 | Rubella model with vaccination solved through Runge-Kutta order 4 and order 5 methods. | Order 5 Runge-Kutta is better than the order 4 Runge-Kutta. Graph of order 5 Runge-Kutta is closer to the results of the analytical simulation. | [14] |
| 13 | Rubella SEIR-V model with vaccination as a control. | If $R_0 < 1$, then Rubella-free equilibrium points are stable. If $R_0 > 1$, then endemic equilibrium points are stable leading to the pitchfork bifurcation, numerical simulations confirm the results of analytical computations. | [15] |

**Table 2:** Summary of key contributions and outcomes from recent Rubella models.

| Sr. No. | Main Contributions | Outcomes | Citation |
|---|---|---|---|
| 1 | Rubella model with ABC operator, simulations utilizing Toufik–Atangana scheme and bifurcation analysis. First study to apply the ABC derivative to the Rubella model with both constant and time-dependent optimal controls. | Time dependent vaccination and treatment reduce infections and associated costs more effectively than constant controls. | [22] |
| 2 | Fractional-order rubella model with vertical transmission incorporating susceptible vaccinated, protected, exposed, infected, and recovered with saturated incidence rate. Grunwald-Letnikov approximation method. | Rubella-free equilibrium point always exists and stable if $R_0 < 1$ , while the endemic equilibrium point exists if $R_0 > 1$, stable if the Routh-Hurwitz criterion is satisfied. | [23] |
| 3 | Rubella model with beta-derivative solved through Sumudu transform. | Outcomes show that the model depends on both parameters and the fractional order. | [24] |
| 4 | Rubella model with fractal fractional operator, parameter estimation using real data. Comparison of error norms revealed that the fractal fractional operator produces the smaller error. | Rise of recovery rate and decline of transmission rate declines the Rubella spread. Vaccination and isolation can help to control Rubella disease. | [25] |
| 5 | Rubella model with ABC fractional derivative solved through Sumudu transform, existence and uniqueness of solution. | Numerical simulations underpin the effectiveness of the ABC derivative. | [26] |
| 6 | Piecewise model incorporating two different kernels with real data. In the first interval, the Caputo operator was employed, while the Atangana–Baleanu derivative was utilized in the second interval, the piecewise numerical Newton polynomial technique. | The utilized approach is effective and flexible in modeling the spread of the Rubella virus. | [27] |

### 1.4. Arrangement of study

The remaining part of the article is arranged as follows: Section 2 presents the formulation and description of the suggested model, which is compressively mathematically and numerically analyzed in Section 3. Section 4 provides the numerical scheme based on Newton polynomials used to solve the suggested system with ABC and FFM operator in section 5. Section 6 concludes the findings of the study.

### 1.5. Basic concepts

In this part, we provide the basic concepts to be utilized in the major part of the article from [28, 29].

**Definition 1:** The Atangana-Baleanu-Caputo (ABC) fractional derivative of order $\tau \in (0,1)$ for a function $f(t)$ is defined as:

$$ {}_0^{ABC}D_t^{\tau} f(t) = \frac{B(\tau)}{1-\tau} \int_0^t f'(\Upsilon) E_{\tau}\left[-\tau \frac{(t-\Upsilon)^{\tau}}{1-\tau}\right] d\Upsilon \tag{1} $$

where $B(\tau)$ is a normalization function satisfying $B(0) = B(1) = 1$, and $E_{\tau}(z)$ is the one-parameter Mittag-Leffler function defined as:

$$ E_{\tau}(z) = \sum_{k=0}^{\infty} \frac{z^k}{\Gamma(\tau k + 1)}, \quad \tau > 0 \tag{2} $$

The Laplace transform of the ABC derivative is:

$$ \mathscr{L}\left\{{}_0^{ABC}D_t^{\tau} f(t)\right\} = \frac{B(\tau)}{1-\tau} \frac{s^{\tau}\mathscr{L}\{f(t)\}(s) - s^{\tau-1}f(0)}{s^{\tau} + \frac{\tau}{1-\tau}} \tag{3} $$

**Definition 2:** The fractal-fractional derivative of order $\tau \in (0,1)$ and fractal dimension $\xi \in (0,1)$ is defined as:

$$ {}_0^{FFM}D_t^{\tau,\xi} f(t) = \frac{B(\tau)}{1-\tau} \frac{d}{dt^{\xi}} \int_0^t f(\Upsilon) E_{\tau}\left[-\tau \frac{(t-\Upsilon)^{\tau}}{1-\tau}\right] d\Upsilon \tag{4} $$

where $\frac{d}{dt^{\xi}}$ denotes the fractal derivative:

$$ \frac{df(t)}{dt^{\xi}} = \lim_{t \to t_1} \frac{f(t) - f(t_1)}{t^{\xi} - t_1^{\xi}}, \quad \xi > 0 \tag{5} $$

The FFM operator can be expressed as:

$$ {}_0^{FFM}D_t^{\tau,\xi} f(t) = \frac{1}{\xi t^{\xi-1}} \cdot {}_0^{ABC}D_t^{\tau} f(t) \tag{6} $$

## 2. Formulation and description of model

In this section, we provide the construction of the Rubella *SVEIR* model that captures the essential dynamics: susceptible individuals can be vaccinated, infected, or die naturally. Vaccinated individuals have reduced susceptibility. Exposed individuals progress to infectiousness and recovered individuals gain lifelong immunity.

We have divided the suggested model into Five compartments: susceptible humans, vaccinated humans, exposed humans, infected humans and recovered humans. $S$ denotes the susceptible individuals, $V$ represents the vaccinated individuals, $E$ is the group of exposed humans, $I$ is the class of infectious humans, $R$ is the group of recovered humans with lifelong immunity. Susceptible humans are recruited at the rate of $\Lambda$, get vaccinated at the rate of $\phi$, die naturally at the rate of $\mu$ and contact with infected humans at the rate of transmission rate $\beta$ to move towards exposed humans. Vaccinated humans get contact with infected humans to move towards exposed class at the transmission rate of $\beta_v$. The exposed humans are decreased by the progression rate $\alpha$. The infected humans are decreased by the recovery rate $\gamma$ and the disease-induced death rate $\delta$ (negligible for rubella, but included for generality). Figure 2 depicts the relationship between the several compartments and model parameters used to create the Rubella model:

**Table 3:** Biological Parameters of Rubella SVEIR Model

| Parameter | Description | Typical Value | Unit |
|---|---|---|---|
| $\Lambda$ | Recruitment rate (births/immigration) | 0.8 | week$^{-1}$ |
| $\beta$ | Transmission rate (susceptible) | 0.008 | week$^{-1}$ |
| $\beta_v$ | Reduced transmission rate (vaccinated) | 0.0008 | week$^{-1}$ |
| $\phi$ | Vaccination rate | 0.015 | week$^{-1}$ |
| $\mu$ | Natural death rate | 0.0005 | week$^{-1}$ |
| $\alpha$ | Progression rate $E \to I$ | 0.5 | week$^{-1}$ |
| $\gamma$ | Recovery rate | 0.33 | week$^{-1}$ |
| $\delta$ | Disease-induced death rate | 0.00005 | week$^{-1}$ |

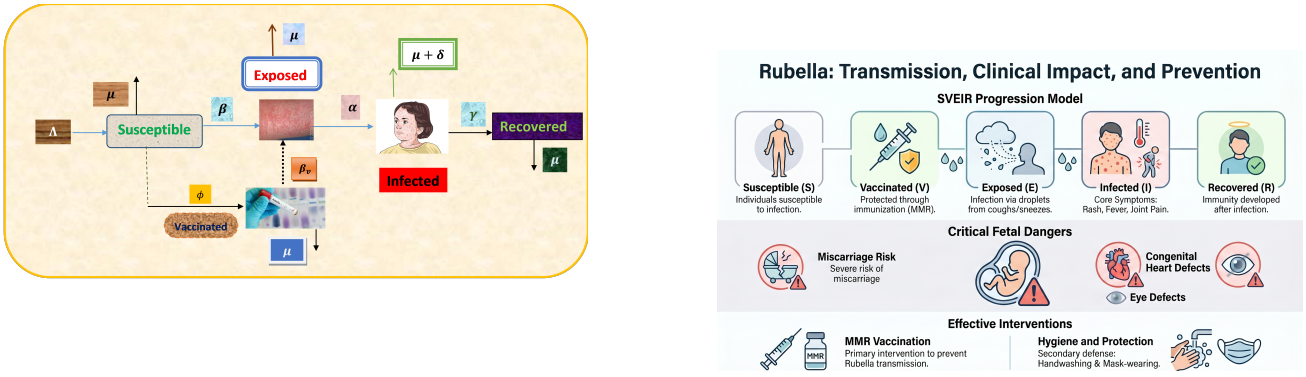


**(a)** **(b)**

**Figure 2:** Schematic diagram of the *SVEIR* Rubella model showing transitions between susceptible, vaccinated, exposed, infected and recovered compartments.

The rubella transmission dynamics are governed by the following system of ordinary differential equations:

$$\begin{cases} \dfrac{dS}{dt} = \Lambda - (\beta I + \mu + \phi)S, \\ \dfrac{dV}{dt} = \phi S - (\beta_v I + \mu)V, \\ \dfrac{dE}{dt} = \beta SI + \beta_v VI - (\alpha + \mu)E, \\ \dfrac{dI}{dt} = \alpha E - (\gamma + \mu + \delta)I, \\ \dfrac{dR}{dt} = \gamma I - \mu R, \end{cases} \tag{7}$$

with initial conditions $S(0) \geq 0, V(0) \geq 0, E(0) \geq 0, I(0) \geq 0, R(0) \geq 0$.

The concept of fractal fractional derivative is introduced by [21], which is a highly helpful tool for tackling challenging issues. The idea on this topic is quite helpful in solving some difficult challenges in many circumstances. Two orders are distinguished for the operator: fractional order and fractal dimension. This approach is superior to the conventional one for the derivation of fractal fractions. Fraction operators and fractal dimensions are responsible for this. Simultaneous investigation is possible when dealing with fractional derivatives that have fractal features. The ability to create a model that more correctly represents a system with a memory effect is one of the operator's many advantages. Furthermore, a lot of real-world problems require an understanding of the amount of information a system possesses. For details, please take a look at references [30].

The fractal fractional extension of the above Rubella model is given by:

$$\begin{aligned}
&{}_0^{FFM}D_t^{\tau,\xi} S = \Lambda - (\beta I + \mu + \phi)S,\\
&{}_0^{FFM}D_t^{\tau,\xi} V = \phi S - (\beta_v I + \mu)V,\\
&{}_0^{FFM}D_t^{\tau,\xi} E = (\beta S + \beta_v V)I - (\alpha_E + \mu)E,\\
&{}_0^{FFM}D_t^{\tau,\xi} I = \alpha_E E - (\gamma + \mu + \delta)I,\\
&{}_0^{FFM}D_t^{\tau,\xi} R = \gamma I - \mu R,
\end{aligned} \tag{8}$$

with initial conditions: $S(0) = S_0 \geq 0, E(0) = E_0 \geq 0, I(0) = I_0 \geq 0, R(0) = R_0 \geq 0, V(0) = V_0 \geq 0$.

## 3. Mathematical analysis of the Rubella model

In this section, we provide comprehensive mathematical analysis of the suggested model including equilibrium points, stability analysis, reproductive number, presence of positive, bounded solution.

### *3.1. Equilibrium points*

The disease-free equilibrium corresponds to the absence of infection. Setting $dE/dt = dI/dt = 0$ and solving:

$$\mathscr{E}_0 = \left(\frac{\Lambda}{\mu+\phi}, = \frac{\phi\Lambda}{\mu(\mu+\phi)}, 0, 0, 0\right), \tag{9}$$

Biologically, at the disease-free equilibrium, the population reaches a steady state where births and deaths balance, and a constant proportion of individuals are vaccinated. The susceptible population $S_0$ decreases with increasing vaccination rate $\phi$, while the vaccinated population $V_0$ increases with $\phi$ but is limited by the natural death rate $\mu$.

**Theorem 1:** If $R_0 > 1$, system (8) has a unique endemic equilibrium $\mathscr{E}^* = (S^*, V^*, E^*, I^*, R^*)$ with $I^* > 0$ given by:

$$\begin{aligned}
S^* &= \frac{\Lambda}{\beta I^* + \mu + \phi},\\
V^* &= \frac{\phi S^*}{\beta_v I^* + \mu},\\
E^* &= \frac{(\gamma + \mu + \delta)I^*}{\alpha},\\
R^* &= \frac{\gamma I^*}{\mu}.
\end{aligned}$$

From $dE/dt = 0$:

$$(\beta S^* + \beta_v V^*)I^* = (\alpha + \mu)E^*.$$

Substitute $E^*$ and $S^*$, $V^*$:

$$\left(\frac{\beta\Lambda}{\beta I^* + \mu + \phi} + \frac{\beta_v \phi \Lambda}{(\beta_v I^* + \mu)(\mu + \phi)}\right) I^* = (\alpha + \mu) \cdot \frac{\gamma + \mu + \delta}{\alpha} I^*.$$

Divide both sides by $I^*$ (since $I^* > 0$):

$$\frac{\beta\Lambda}{\beta I^* + \mu + \phi} + \frac{\beta_v \phi \Lambda}{(\beta_v I^* + \mu)(\mu + \phi)} = \frac{(\alpha + \mu)(\gamma + \mu + \delta)}{\alpha}.$$

Multiply both sides by $(\beta I^* + \mu + \phi)(\beta_v I^* + \mu)(\mu + \phi)$ and simplify to obtain:

$$\beta\beta_v (I^*)^2 + \left[\beta\mu + \beta_v(\mu + \phi) - \frac{\alpha\beta_v\Lambda}{(\alpha + \mu)(\gamma + \mu + \delta)}\right] I^* + \mu(\mu + \phi)\left(1 - \frac{1}{R_0}\right) = 0.$$

This is exactly $A(I^*)^2 + BI^* + C = 0$ with $A, B, C$ as defined. When $R_0 > 1$, $C < 0$, so exactly one positive root exists.

This equilibrium represents the baseline rubella incidence in the absence of control measures or seasonal forcing. The stability of the endemic equilibrium depends on the recovery rate $\gamma$ and transmission rate $\beta$.

*3.2. Basic reproduction number*

In this part, we compute the reproductive number using next-generation matrix method. The basic reproduction number $R_0$ is the expected number of secondary infections caused by a single infectious individual in a completely susceptible population. We compute $R_0$ using the next-generation matrix method [31].

First, identify infectious compartments $E$ (exposed) and $I$ (infectious). Then, construct $\mathscr{F}$ and $\mathscr{V}$ matrices

$$\mathscr{F} = \begin{pmatrix} \beta SI + \beta_v VI \\ 0 \end{pmatrix}, \quad \mathscr{V} = \begin{pmatrix} (\alpha+\mu)E \\ -\alpha E + (\gamma+\mu+\delta)I \end{pmatrix}.$$

Here, $\mathscr{F}$ represents the rate of new infections entering each compartment, and $\mathscr{V}$ represents the rate of other transitions. Now, compute jacobian at Rubella-free equilibrium point:

$$F = \left.\frac{\partial \mathscr{F}}{\partial (E,I)}\right|_{\mathscr{E}_0} = \begin{pmatrix} 0 & \beta S_0 + \beta_v V_0 \\ 0 & 0 \end{pmatrix},$$

$$V = \left.\frac{\partial \mathscr{V}}{\partial (E,I)}\right|_{\mathscr{E}_0} = \begin{pmatrix} \alpha+\mu & 0 \\ -\alpha & \gamma+\mu+\delta \end{pmatrix}.$$

The inverse of $V$ is:

$$V^{-1} = \frac{1}{(\alpha+\mu)(\gamma+\mu+\delta)} \begin{pmatrix} \gamma+\mu+\delta & 0 \\ \alpha & \alpha+\mu \end{pmatrix}.$$

The next-generation matrix $K = FV^{-1}$ is:

$$K = \frac{1}{(\alpha+\mu)(\gamma+\mu+\delta)} \begin{pmatrix} \alpha(\beta S_0 + \beta_v V_0) & 0 \\ 0 & 0 \end{pmatrix}.$$

Reproductive number $R_0$ is the spectral radius of $K$ given by:

$$\boxed{R_0 = \frac{\alpha\Lambda}{(\alpha+\mu)(\gamma+\mu+\delta)} \left( \frac{\beta}{\mu+\phi} + \frac{\beta_v \phi}{\mu(\mu+\phi)} \right)}.$$

*3.3. Stability of equilibrium points*

**Theorem 2:** If $R_0 < 1$, the disease-free equilibrium $\mathscr{E}_0$ is locally asymptotically stable. If $R_0 > 1$, $\mathscr{E}_0$ is unstable.

**Proof:**

$$J = \begin{pmatrix} -(\beta I + \mu + \phi) & 0 & 0 & -\beta S & 0 \\ \phi & -(\beta_v I + \mu) & 0 & -\beta_v V & 0 \\ \beta I & \beta_v I & -(\alpha+\mu) & \beta S + \beta_v V & 0 \\ 0 & 0 & \alpha & -(\gamma+\mu+\delta) & 0 \\ 0 & 0 & 0 & \gamma & -\mu \end{pmatrix}.$$

At the disease-free equilibrium $\mathscr{E}_0$, the Jacobian simplifies to:

$$J(\mathscr{E}_0) = \begin{pmatrix} -(\mu+\phi) & 0 & 0 & -\beta S_0 & 0 \\ \phi & -\mu & 0 & -\beta_v V_0 & 0 \\ 0 & 0 & -(\alpha+\mu) & \beta S_0 + \beta_v V_0 & 0 \\ 0 & 0 & \alpha & -(\gamma+\mu+\delta) & 0 \\ 0 & 0 & 0 & \gamma & -\mu \end{pmatrix}.$$

The eigenvalues of $J(\mathscr{E}_0)$ are:

$$\lambda_1 = -\mu \quad (\text{multiplicity } 2), \lambda_2 = -(\mu+\phi),$$

$$\lambda_{3,4} = \frac{-[(\alpha+\mu)+(\gamma+\mu+\delta)] \pm \sqrt{[(\alpha+\mu)-(\gamma+\mu+\delta)]^2 + 4\alpha(\beta S_0 + \beta_v V_0)}}{2}.$$

All eigenvalues have negative real parts if and only if the real parts of $\lambda_{3,4}$ are negative. This occurs when:

$$(\alpha+\mu)(\gamma+\mu+\delta) > \alpha(\beta S_0 + \beta_v V_0) \iff R_0 < 1.$$

Thus, the Rubella-free equilibrium points is locally asymptotically stable when $R_0 < 1$ and unstable when $R_0 > 1$. All eigenvalues have negative real parts, meaning small perturbations (e.g., a single imported rubella case) decay exponentially. Rubella can be eliminated regionally if vaccination coverage maintains $R_0 < 1$. The local stability analysis shows that once $R_0$ is pushed below 1, rubella elimination is robust to small perturbations. Even when $R_0 > 1$, the system may return to equilibrium after an outbreak (damped oscillations).

*3.4. Global stability of Rubella-free equilibrium points*

For the disease-free equilibrium, we construct a Lyapunov function to prove global stability.

**Theorem 3:** If $R_0 < 1$, the disease-free equilibrium $\mathscr{E}_0$ is globally asymptotically stable.

**Proof:** Consider the Lyapunov function candidate:

$$L(E,I) = \frac{1}{2}E^2 + \frac{\alpha}{2(\gamma+\mu+\delta)}I^2. \tag{10}$$

The time derivative along trajectories is:

$$\begin{aligned}
\dot{L} &= E\dot{E} + \frac{\alpha}{\gamma+\mu+\delta}I\dot{I} \\
&= E[(\beta S + \beta_v V)I - (\alpha+\mu)E] + \frac{\alpha}{\gamma+\mu+\delta}I[\alpha E - (\gamma+\mu+\delta)I] \\
&= -(\alpha+\mu)E^2 - \alpha I^2 + \alpha EI + \frac{\alpha^2}{\gamma+\mu+\delta}EI \\
&= -(\alpha+\mu)E^2 - \alpha I^2 + \alpha EI\left[1 + \frac{\alpha}{\gamma+\mu+\delta}\right].
\end{aligned}$$

Using the inequality $2EI \le E^2 + I^2$, we obtain:

$$\dot{L} \le -(\alpha+\mu)E^2 - \alpha I^2 + \frac{\alpha}{2}\left(1 + \frac{\alpha}{\gamma+\mu+\delta}\right)(E^2+I^2). \tag{11}$$

This can be written as $\dot{L} \le -(1-R_0)(\text{positive terms}) \le 0$ when $R_0 \le 1$. By LaSalle's invariance principle, all trajectories converge to the largest invariant set where $\dot{L} = 0$, which is $\mathscr{E}_0$.

**Biological interpretation:** The Lyapunov function method shows that rubella elimination is not just locally stable but globally stable when $R_0 \le 1$. This means that regardless of the initial number of infectious individuals, the disease will eventually die out if the basic reproduction number is below unity.

*3.5. Boundedness and Positivity of Solutions*

We first show that all solutions of the rubella SVEIR model remain non-negative and bounded.

**Integer-order case:** For the classical model (ordinary derivatives) we have, for all $t \ge 0$,

$$\begin{aligned}
&S(t) \ge S(0)\,e^{-(\beta\|I\|_\infty+\mu+\phi)t}, \quad V(t) \ge V(0)\,e^{-(\beta_v\|I\|_\infty+\mu)t}, \\
&E(t) \ge E(0)\,e^{-(\alpha+\mu)t}, \qquad I(t) \ge I(0)\,e^{-(\gamma+\mu+\delta)t}, \qquad R(t) \ge R(0)\,e^{-\mu t}.
\end{aligned}$$

**Fractal-fractional (FFM) case:** Using the Caputo-type FFM derivative of order $\tau$ and fractal dimension $\xi$, we obtain the estimates

$$\begin{aligned}
S(t) &\ge S(0)\,E_\tau\left[-\frac{\delta^{1-\xi}\tau(\beta I+\mu+\phi)t^\tau}{AB(\tau)-(1-\tau)(\beta I+\mu+\phi)}\right], \\
E(t) &\ge E(0)\,E_\tau\left[-\frac{\delta^{1-\xi}\tau(\alpha+\mu)t^\tau}{AB(\tau)-(1-\tau)(\alpha+\mu)}\right], \\
I(t) &\ge I(0)\,E_\tau\left[-\frac{\delta^{1-\xi}\tau(\gamma+\mu+\delta)t^\tau}{AB(\tau)-(1-\tau)(\gamma+\mu+\delta)}\right], \\
R(t) &\ge R(0)\,E_\tau\left[-\frac{\delta^{1-\xi}\tau\mu t^\tau}{AB(\tau)-(1-\tau)\mu}\right], \\
V(t) &\ge V(0)\,E_\tau\left[-\frac{\delta^{1-\xi}\tau\mu t^\tau}{AB(\tau)-(1-\tau)\mu}\right],
\end{aligned}$$

where $E_\tau$ is the Mittag-Leffler function and $AB(\tau) = 1-\tau+\frac{\tau}{\Gamma(\tau)}$ is the normalization function.

*3.6. Positively Invariant Region*

Define the total population $N(t) = S(t)+V(t)+E(t)+I(t)+R(t)$. From the model equations we have

$$\frac{dN}{dt} = \Lambda - \mu N - \delta I \leq \Lambda - \mu N.$$

Hence $\limsup_{t\to\infty} N(t) \leq \Lambda/\mu$. The set

$$\Omega = \left\{ (S,V,E,I,R) \in \mathbb{R}^5_+ : \; S+V+E+I+R \leq \frac{\Lambda}{\mu} \right\}$$

is positively invariant and attracting.

**Lemma 1:** The region

$$\Gamma = \left\{ (S,V,E,I,R) \in \mathbb{R}^5_+ : \; 0 \leq N(t) \leq \frac{\Lambda}{\mu} \right\}$$

is positively invariant under non-negative initial conditions and attracts all solutions.

**Proof:** On the boundary of $\mathbb{R}^5_+$ the vector field points inward (all derivatives are non-negative). Summing the five equations gives

$${}^{FFM}D^{\tau,\xi}_{0,t} N(t) = \Lambda - \mu N(t) - \delta I(t) \leq \Lambda - \mu N(t).$$

Solving this inequality yields $N(t) \leq \Lambda/\mu$ for all $t \geq 0$ if initially $N(0) \leq \Lambda/\mu$. Thus $\Gamma$ is positively invariant.

**Remark 1:** Lemma 1 guarantees that all biologically meaningful solutions remain non-negative and bounded, ensuring the model is well-posed.

*3.7. Existence and uniqueness of solutions*

Rewrite the FFM system in the compact form

$${}^{FFM}D^{\tau,\xi}_{0,t} X(t) = F(t,X(t)), \qquad X(0) = X_0,$$

where $X = (S,V,E,I,R)$ and the components of $F$ are

$$\begin{aligned}
F_S &= \Lambda - (\beta I + \mu + \phi)S, \\
F_V &= \phi S - (\beta_v I + \mu)V, \\
F_E &= (\beta S + \beta_v V)I - (\alpha + \mu)E, \\
F_I &= \alpha E - (\gamma + \mu + \delta)I, \\
F_R &= \gamma I - \mu R.
\end{aligned}$$

Using the equivalent integral form of the FFM derivative,

$$X(t) = X(0) + \frac{\xi(1-\tau)t^{\xi-1}}{AB(\tau)} F(t,X(t)) + \frac{\tau\xi}{AB(\tau)\Gamma(\tau)} \int_0^t (t-\delta)^{\tau-1} \delta^{\xi-1} F(\delta,X(\delta))\, d\delta,$$

we split the operator into a contraction part $\mathscr{Q}$ (local Lipschitz terms) and a compact part $\mathscr{W}$ (integral term). By showing that $\mathscr{Q}$ is a contraction and $\mathscr{W}$ is completely continuous, Krasnoselskii's fixed point theorem guarantees the existence of a unique local solution. Positivity and boundedness then extend it globally.

*3.8. Stability Analysis of the Endemic Equilibrium*

Assume $R_0 > 1$ so that a unique endemic equilibrium $X^* = (S^*,V^*,E^*,I^*,R^*)$ exists.

**Lemma 2:** For any constant $U^* > 0$ and for all $t \geq 0$,

$${}^{FFM}D^{\tau,\xi}_{0,t} \left( U(t) - U^* - U^* \ln \frac{U(t)}{U^*} \right) \leq \left( 1 - \frac{U^*}{U(t)} \right)^{FFM} D^{\tau,\xi}_{0,t} U(t).$$

**Theorem 4:** If $R_0 > 1$, the endemic equilibrium $X^*$ is globally asymptotically stable.

**Proof:** Consider the Lyapunov functional

$$\mathscr{U}(t) = \sum_{i=1}^{5} \left( X_i(t) - X_i^* - X_i^* \ln \frac{X_i(t)}{X_i^*} \right),$$

where $X_1 = S$, $X_2 = V$, $X_3 = E$, $X_4 = I$, $X_5 = R$. Applying Lemma 2 and the model equations, we obtain after rearrangement

$${}^{FFM}D_{0,t}^{\tau,\xi}\mathscr{U}(t) \leq \Theta_x - \Theta_y,$$

with

$$\begin{aligned}
\Theta_x &= \Lambda + \nu(S - S^*) + \zeta(E - E^*) + \mu(I - I^*) + \eta(V - V^*), \\
\Theta_y &= \Lambda \frac{S^*}{S} + (\nu + \sigma + \omega)\frac{(S - S^*)^2}{S} + (\zeta + \omega)\frac{(E - E^*)^2}{E} + (\mu + \omega)\frac{(I - I^*)^2}{I} \\
&\quad + \omega\frac{(R - R^*)^2}{R} + \omega\frac{(V - V^*)^2}{V} + \text{cross terms}.
\end{aligned}$$

One can show $\Theta_y \geq \Theta_x$ with equality only at $X = X^*$. Hence

$${}^{FFM}D_{0,t}^{\tau,\xi}\mathscr{U}(t) \leq 0,$$

and by LaSalle's invariance principle, $X^*$ is globally asymptotically stable.

Now, we compute the Second derivative of the Lyapunov function. To further characterise the convergence, we compute the fractional derivative of $\dot{\mathscr{U}}$:

$${}^{FFM}D_{0,t}^{\tau,\xi}\left[{}^{FFM}D_{0,t}^{\tau,\xi}\mathscr{U}(t)\right] = \Lambda_1 - \Lambda_2.$$

The sign of this expression determines the acceleration of the approach to equilibrium:

$$\begin{aligned}
\Lambda_1 > \Lambda_2 &\implies \text{convex decay (faster convergence)}, \\
\Lambda_1 < \Lambda_2 &\implies \text{concave decay (slower convergence)}, \\
\Lambda_1 = \Lambda_2 &\implies \text{linear decay}.
\end{aligned}$$

The fractal fractional-order SVEIR model possesses a unique, non-negative, bounded solution. The disease-free equilibrium is stable when $R_0 < 1$; the endemic equilibrium is globally asymptotically stable when $R_0 > 1$. The Lyapunov analysis confirms that the memory effects (via the FFM derivative) do not alter the long-term stability, only the transient dynamics.

### *3.9. Transcritical bifurcation analysis*

A transcritical bifurcation occurs when a trivial equilibrium and a nontrivial equilibrium exchange stability as a parameter crosses a critical value. Here, the disease-free equilibrium $\mathscr{E}_0$ and endemic equilibrium $\mathscr{E}^*$ collide and swap stability at $R_0 = 1$.

**Theorem 5:** Consider system (8) with $\beta$ as bifurcation parameter. At $\beta = \beta^*$ defined by $R_0(\beta^*) = 1$, there exists a transcritical bifurcation. For $\beta < \beta^*$ ($R_0 < 1$), the disease-free equilibrium $\mathscr{E}_0$ is locally asymptotically stable. For $\beta > \beta^*$ ($R_0 > 1$), $\mathscr{E}_0$ becomes unstable and a stable endemic equilibrium $\mathscr{E}^*$ appears.

**Proof:** We follow the approach of [32].

In the First step, we select $\beta$ as the bifurcation parameter. At $R_0 = 1$, from reproductive number, we obtain the following expression:

$$\frac{\alpha(\beta^* S_0 + \beta_v V_0)}{(\alpha + \mu)(\gamma + \mu + \delta)} = 1.$$

Solving for $\beta^*$, we obtain:

$$\beta^* S_0 + \beta_v V_0 = \frac{(\alpha + \mu)(\gamma + \mu + \delta)}{\alpha}.$$

Thus:

$$\beta^* = \frac{(\alpha + \mu)(\gamma + \mu + \delta)}{\alpha S_0} - \frac{\beta_v V_0}{S_0}. \tag{12}$$

In the Second step, shift the disease-free equilibrium to the origin by defining:

$$x_1 = E, x_2 = I, x_3 = S - S_0, x_4 = V - V_0, x_5 = R.$$

Then the Rubella-free equilibrium point become $x = 0$. Let $\phi = \beta - \beta^*$ be the bifurcation parameter deviation, so that $\phi = 0$ at the bifurcation point.

At $\beta = \beta^*$ ($\phi = 0$), the Jacobian $J(\mathscr{E}_0)$ at Rubella-free equilibrium points has One simple zero eigenvalue, Four eigenvalues with negative real parts (since $R_0 = 1$ at bifurcation).

The presence of a simple zero eigenvalue satisfies the conditions for center manifold theory.

The right eigenvector $v = (v_1, v_2, v_3, v_4, v_5)^T$ satisfies $J(\mathscr{E}_0)v = 0$:

The right eigenvector is:

$$v = \begin{pmatrix} v_1 \\ v_2 \\ v_3 \\ v_4 \\ v_5 \end{pmatrix} = \begin{pmatrix} \frac{\gamma+\mu+\delta}{\alpha} \\ 1 \\ -\frac{\beta^* S_0}{\mu+\phi} \\ -\frac{\beta_v V_0}{\mu} \\ \frac{\gamma}{\mu} \end{pmatrix}. \tag{13}$$

The left eigenvector $w = (w_1, w_2, w_3, w_4, w_5)$ satisfies $wJ(\mathscr{E}_0) = 0$.

Thus, the normalized left eigenvector is:

$$\boxed{w = \begin{pmatrix} w_1 \\ w_2 \\ w_3 \\ w_4 \\ w_5 \end{pmatrix} = \begin{pmatrix} \frac{\alpha}{\alpha+\gamma+2\mu+\delta} \\ \frac{\alpha+\mu}{\alpha+\gamma+2\mu+\delta} \\ 0 \\ 0 \\ 0 \end{pmatrix}.} \tag{14}$$

Now, we compute bifurcation coefficients defined as:

$$a = \sum_{k,i,j=1}^{n} w_k v_i v_j \frac{\partial^2 f_k}{\partial x_i \partial x_j}(0,0), \qquad b = \sum_{k,i=1}^{n} w_k v_i \frac{\partial^2 f_k}{\partial x_i \partial \beta}(0,0). \tag{15}$$

$$\boxed{b = \frac{\alpha S_0}{\alpha+\gamma+2\mu+\delta} > 0}. \tag{16}$$

$$a = 2w_1 \left( \frac{(\beta^*)^2 S_0}{\mu+\phi} + \frac{\beta_v^2 V_0}{\mu} \right) > 0.$$

Then with $a > 0$ and $b > 0$, the bifurcation is transcritical and the endemic equilibrium is locally asymptotically stable for $\beta > \beta^*$ ($R_0 > 1$). Thus, we conclude:

$$a = 2w_1 \left( \frac{(\beta^*)^2 S_0}{\mu+\phi} + \frac{\beta_v^2 V_0}{\mu} \right) > 0, \quad b = \frac{\alpha S_0}{\alpha+\gamma+2\mu+\delta} > 0. \tag{17}$$

Since $a > 0$ and $b > 0$, a transcritical bifurcation occurs at $\beta = \beta^*$ ($\phi = 0$). The disease-free equilibrium $\mathscr{E}_0$ is locally asymptotically stable for $\beta < \beta^*$ ($R_0 < 1$). The disease-free equilibrium $\mathscr{E}_0$ is unstable for $\beta > \beta^*$ ($R_0 > 1$). A unique endemic equilibrium $\mathscr{E}^*$ exists and is locally asymptotically stable for $\beta > \beta^*$ ($R_0 > 1$).

**Biological interpretation:** The transcritical bifurcation at $R_0 = 1$ represents the invasion threshold for rubella: When $R_0 < 1$: The disease cannot sustain itself in the population. A small number of imported rubella cases will die out without causing an outbreak. This is the elimination regime. Public health efforts should aim to keep $R_0 < 1$ through vaccination. When $R_0 > 1$: Rubella can establish itself in the population, leading to an endemic state. This is the persistence regime. Even with vaccination, rubella may continue to circulate, requiring ongoing control measures. From $R_0 = 1$, solving for $\phi$ gives the critical vaccination rate needed for elimination. For high vaccine efficacy ($\beta_v \ll \beta$), we have:

$$\phi_c \approx \frac{\mu(\alpha+\mu)(\gamma+\mu+\delta)}{\alpha\Lambda} \cdot \frac{\beta}{\beta - \beta_v} \cdot (\beta S_0 + \beta_v V_0). \tag{18}$$

For rubella, this typically requires approximately $80-85\%$ lifetime vaccination coverage with two doses of MMR vaccine. Vaccination rate $\phi$ directly lowers $R_0$ (appears in the denominator of $S_0$). Higher vaccination rates reduce the susceptible population, making it harder for rubella to persist.

Based on the transcritical bifurcation analysis, the following public health recommendations emerge: Maintain vaccination coverage such that $R_0 < 1$ to achieve rubella elimination. For rubella, this requires approximately $80-85\%$ coverage with a two-dose MMR schedule. When $R_0 > 1$ (e.g., due to waning immunity or vaccine refusal), aggressive outbreak response (mass vaccination campaigns, contact tracing) is needed to push $R_0$ back below 1. Estimate $R_0$ regularly from case data to determine if rubella is in elimination or endemic regime. A sudden increase in reported cases may indicate $R_0$ has crossed the threshold. The critical vaccination coverage $\phi_c$ defines the herd immunity threshold. For rubella, this threshold is achievable with routine childhood immunization.

### *3.10. Chaos analysis using the 0-1 test*

The 0-1 chaos test is a binary test that distinguishes between regular and chaotic dynamics in dynamical systems without requiring phase space reconstruction [33, 34]. Unlike Lyapunov exponent calculations, this test works directly on time series data and is robust to noise.

For a time series $\phi(j)$ where $j = 1,2,\ldots,N$, the 0-1 test computes the following transformed coordinates:

$$p(n) = \sum_{j=1}^{n} \phi(j)\cos(jc), \quad q(n) = \sum_{j=1}^{n} \phi(j)\sin(jc)$$

where $c$ is a random constant in $(0,\pi)$, typically taken as $c = \pi/5$ to $2\pi/3$ for robustness. The mean square displacement is then calculated as:

$$M(n) = \lim_{N\to\infty} \frac{1}{N} \sum_{j=1}^{N} \left[(p(j+n)-p(j))^2 + (q(j+n)-q(j))^2\right] \tag{19}$$

The asymptotic growth rate $K$ is determined via correlation or regression:

$$K = \lim_{n\to\infty} \frac{\log M(n)}{\log n} \tag{20}$$

For regular dynamics, $M(n)$ grows slowly and $K \approx 0$; for chaotic dynamics, $M(n)$ grows linearly and $K \approx 1$. In this study, we used multiple $c$ values ($\pi/5, \pi/4, \pi/3, \pi/2, 2\pi/3$) and reported the median $K$ value for robustness. Classification thresholds are set as $K \leq 0.2$: Regular dynamics, $0.2 < K \leq 0.5$: weak chaos (intermittent behavior), $0.5 < K \leq 0.8$: moderate chaos, $K > 0.8$: Strong chaos (deterministic chaos).

For the rubella SVEIR model analyzed here, the 0-1 chaos test is applied to each compartment's steady-state time series. The results are summarized in Figures given below. The 0-1 chaos test revealed that the rubella SVEIR model exhibits compartment-dependent dynamical behavior. All the compartments showed the regular behaviour ($K = 0$). Biologically, the absence of chaos in rubella transmission dynamics has significant epidemiological implications. Absence of chaotic dynamics indicate that the disease incidence exhibits regular. This means traditional forecasting methods will work. Regular dynamics imply that well-designed intervention strategies (e.g., pulse vaccination) can control disease and as a result, the disease can be eliminated very soon in the future.

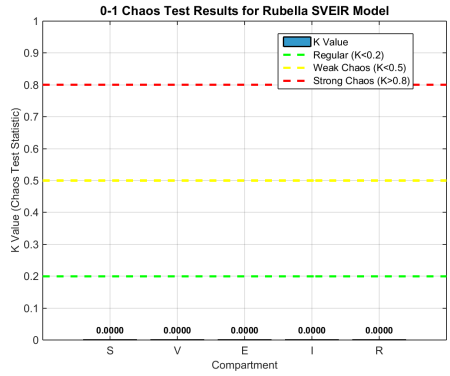


**(a)** Bar chart showing K values for all five compartments with classification thresholds.

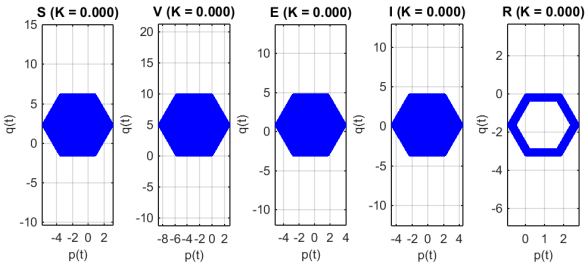


**(b)** p-q plots for all five compartments from the 0-1 chaos test. Regular dynamics produce bounded trajectories.

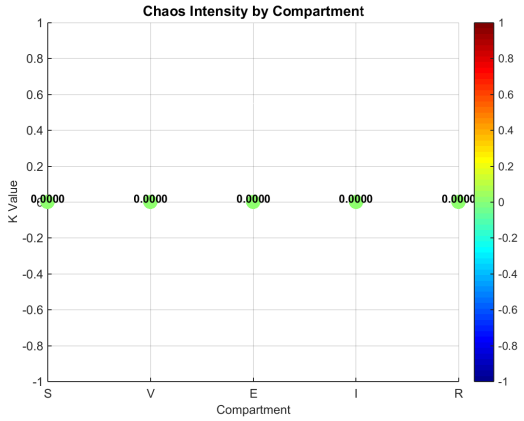


**(c)** Scatter plot showing the K value for each compartment.

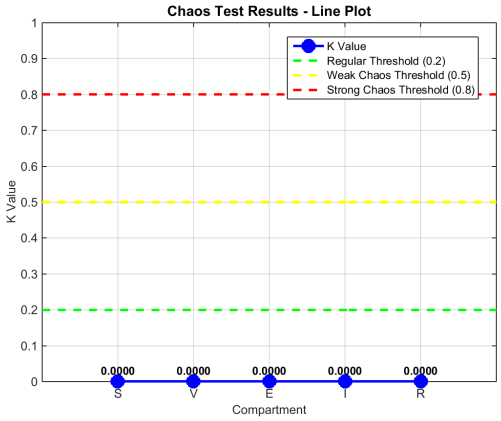


**(d)** Line plot of K values across compartments with threshold lines for classification.

**Figure 3:** Plots showing that all compartments of the suggested model show bounded behaviour.

### *3.11. Statistical analysis*

To quantify the long-term behaviour of the rubella transmission model, a statistical analysis is performed on the steady-state dynamics of each compartment. After discarding the initial transient, the last 500 weeks are treated as stationary data. For all compartments, we compute mean, median, mode, standard deviation, variance, range, interquartile range (IQR), coefficient of variation, skewness and kurtosis. The results are visualised in Figures 4a–4e, each showing the histogram, boxplot and Q-Q plot against the normal distribution. Figure 4a presents the statistical analysis for susceptible humans. The plot illustrates that the histogram is slightly left-skewed and platykurtic, indicating a flatter distribution than normal. The boxplot shows a compact interquartile range and few outliers. The Q-Q plot reveals deviations from normality, especially in the lower tail, reflecting the effect of infection events that deplete the susceptible pool. Figure 4b depicts the statistical analysis for vaccinated humans. Vaccinated individuals accumulate over time, reaching a mean but with very high dispersion, a consequence of the interplay between vaccination rate and natural death. The distribution is right-skewed and slightly leptokurtic. The boxplot exhibits a wide IQR and many outliers, indicating that vaccination coverage can vary substantially depending on the timing of outbreaks. The Q-Q plot confirms non-normality. Figure 4c reflecting the statistical analysis for exposed humans. Nearly all values are zero, reflecting rapid progression to infectious stage. The histogram shows a strong positive skew and extreme kurtosis, indicating rare, brief exposures. The exposed population is extremely low because the latent period of rubella is short. The distribution is strongly right-skewed and highly leptokurtic, reflecting rare, brief spikes in exposure. The boxplot collapses to zero, and the Q-Q plot shows heavy tails typical for a rarely occupied compartment. Figure 4d presents the statistical analysis for infected humans. The infectious population remains near zero with occasional small outbreaks. The

skewness and kurtosis are almost identical to those of exposed humans, confirming that the infectious period is too short to allow accumulation. The Q-Q plot again shows extreme tail behaviour, characteristic of sub-critical epidemic dynamics. Figure 4e reveals the statistical analysis for recovered humans. Recovered individuals accumulate to a steady mean, with low dispersion. The distribution is slightly left-skewed and platykurtic . The boxplot shows a narrow IQR, and the Q-Q plot follows the normal line reasonably well in the central region, though the tails deviate. This indicates that the recovery process is relatively stable once the system reaches equilibrium.

The statistical analysis confirms the infection remains endemic but at a very low level, with most individuals either vaccinated or recovered. The high variability of the vaccinated compartment underscores the importance of continuous vaccination coverage, while the near-zero exposed and infectious compartments reflect the short timescales of the disease progression.

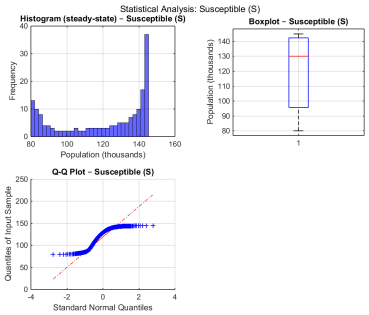


**(a)** Statistical analysis for susceptible humans.

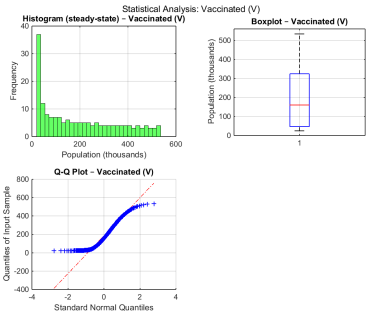


**(b)** Statistical analysis for vaccinated humans.

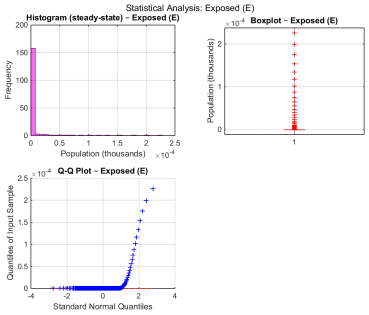


**(c)** Statistical analysis for exposed humans.

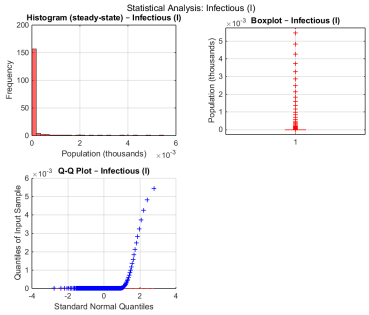


**(d)** Statistical analysis for infected humans.

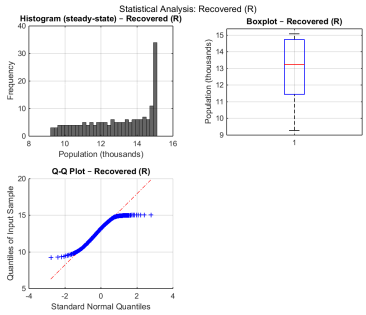


**(e)** Statistical analysis for recovered humans.

**Figure 4:** Statistical analysis for all compartments of the model.

### *3.12. Impact of parameters*

To understand how variations in key epidemiological parameters affect each compartment of the Rubella SVEIR model, a comprehensive 3D parameter analysis is performed. For each compartment, two parameters were simultaneously varied over biologically realistic ranges while keeping all other parameters fixed at baseline values. The resulting 3D bar plots visualize the population responses, providing insights into parameter sensitivity and control strategies.

Figure 5a shows that increasing the transmission rate $\beta$ leads to a decrease in susceptible population because more individuals become infected and leave the susceptible class. This figure also demonstrates that increasing the vaccination rate $\phi$ similarly reduces the susceptible population as more individuals are vaccinated and move to the V compartment. The lowest susceptible population occurs when both $\beta$ and $\phi$ are high, indicating that rubella transmission is maximally suppressed under high vaccination coverage even with high transmission rates. Biologically, this confirms that vaccination is an effective control measure: even at moderate transmission rates, increasing $\phi$ reduces S. Figure 5b shows that increasing the vaccination rate $\phi$ dramatically increases the vaccinated population, which is expected as more susceptible individuals receive vaccination. The plot demonstrates that the natural death rate $\mu$ has a relatively weaker effect on V compared to $\phi$. Higher $\mu$ slightly reduces the vaccinated population due to increased mortality. The maximum vaccinated population is achieved at high $\phi$ and low $\mu$, indicating that vaccination campaigns are most effective in populations with lower mortality rates. Biologically, the plot reveals that vaccination coverage is the primary driver of V, while natural death rate plays a secondary role, suggesting that public health efforts should focus on increasing vaccine uptake rather than reducing mortality. Figure 5c demonstrates that increasing the progression rate $\alpha$ decreases the exposed population because exposed individuals progress to the infectious stage more rapidly. The highest peak of exposed individuals occurs at high $\beta$ and low $\alpha$ ($< 0.4$), representing a situation where rubella spreads easily but has a long latent period. Biologically, the plot indicates that the latent period of rubella is already near the optimal range where exposed populations are moderately controlled. Reducing the latent period would further decrease E, but this is biologically constrained. Figure 5d shows that increasing the transmission rate $\beta$ drastically increases the peak infectious population. The plot demonstrates that increasing the recovery rate $\gamma$ significantly reduces the peak infectious population because infected individuals recover faster, shortening the infectious period. The interaction effect in this figure is striking at low $\beta$, the infectious population remains low regardless of $\gamma$. However, at high $\beta$, increasing $\gamma$ reduces I, showing that treatment and rapid recovery are critical control measures during high-transmission scenarios. Biologically, this plot provides the most important public health insight: for rubella control, reducing transmission (via isolation, hygiene, or vaccination) and increasing recovery (via supportive care) act to lower peak infectious cases. The red plateau at high $\beta$ and low $\gamma$ represents the worst-case outbreak scenario. Figure 5e shows that increasing the recovery rate $\gamma$ increases the recovered population as more infected individuals successfully recover and gain lifelong immunity. The plot demonstrates that increasing the death rate $\mu$ decreases the recovered population because individuals die before reaching the recovered compartment. The maximum recovered population occurs at high $\gamma$ and low $\mu$, representing a scenario where rubella infection leads to high survival and immunity. Biologically, this figure confirms that rubella's lifelong immunity is a key feature: once individuals recover, they remain in the R compartment indefinitely unless death occurs. This explains why rubella elimination is achievable with high vaccination coverage.

## 4. Newton polynomial based numerical scheme

In this part, we aim to provide the numerical scheme based on Newton polynomials for both FFM and ABC operators. The Newton polynomial based schemes are more accurate than those based on Lagrange interpolation (e.g. Adams-Bashforth) because they use higher-order interpolation and better capture the memory effects inherent in fractional operators. These schemes have been successfully applied to several infectious disease models [35, 36].

### *4.1. Numerical scheme for system with FFM operator*

For the rubella SVEIR model we consider the FFM formulation:

$$
\begin{aligned}
{}^{FFM}D_{0,t}^{\tau,\xi}S(t) &= \Lambda-(\beta I+\mu+\phi)S,\\
{}^{FFM}D_{0,t}^{\tau,\xi}V(t) &= \phi S-(\beta_v I+\mu)V,\\
{}^{FFM}D_{0,t}^{\tau,\xi}E(t) &= (\beta S+\beta_v V)I-(\alpha+\mu)E,\\
{}^{FFM}D_{0,t}^{\tau,\xi}I(t) &= \alpha E-(\gamma+\mu+\delta)I,\\
{}^{FFM}D_{0,t}^{\tau,\xi}R(t) &= \gamma I-\mu R,
\end{aligned}
$$

where ${}^{FFM}D_{0,t}^{\tau,\xi}$ denotes the Caputo-type fractal-fractional derivative of order $\tau$ and fractal dimension $\xi$. For compactness we write

$$
{}^{FFM}D_{0,t}^{\tau,\xi}U(t)=\mathscr{D}(t,U(t)),\qquad U=(S,V,E,I,R).
$$

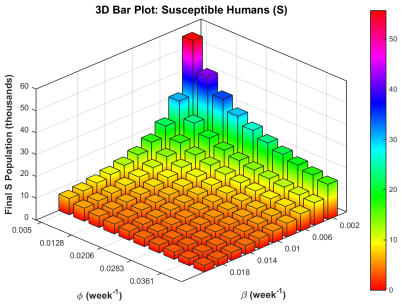


**(a)** Impact of vaccination and transmission rate on susceptible compartment

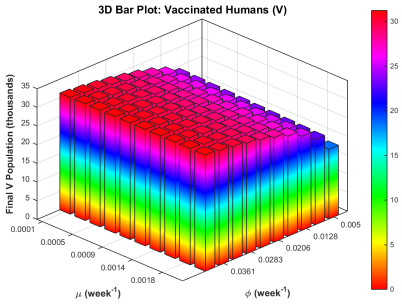


**(b)** Impact of vaccination and natural mortality rate on vaccinated humans compartment

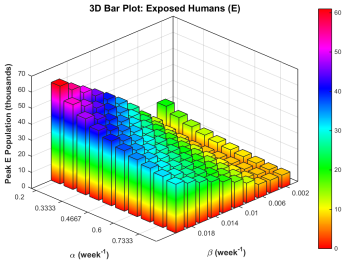


**(c)** Impact of transmission rate and progression rate on exposed humans compartment.

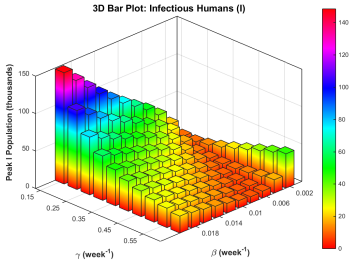


**(d)** Impact of transmission rate and recovery rate on infectious humans compartment.

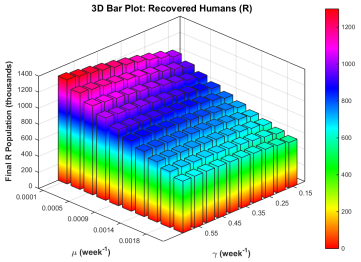


**(e)** Impact of recovery rate and natural mortality rate on recovered humans compartment

**Figure 5:** 3D parameter impact analysis for all compartments of the Rubella SVEIR model. Each subfigure shows how varying two key parameters affects the compartment population.

Using the integral reformulation of the FFM derivative and the Newton polynomial interpolation of $\mathscr{D}(t,U(t))$ on three successive points, we obtain the following discrete scheme for any compartment (here shown for $S$):

$$
\begin{aligned}
S_{n+1} = S(0) &+ \frac{(1-\tau)}{AB(\tau)} t_n^{1-\xi}\, \mathscr{D}_S(t_n,U_n) + \frac{\tau(\Delta t)^\tau}{AB(\tau)\Gamma(\tau+1)} \sum_{q=2}^{n} \mathscr{D}_S(t_{q-2},U_{q-2})\, t_{q-2}^{1-\xi}\, \mathscr{A}_1(n,q) \\
&+ \frac{\tau(\Delta t)^\tau}{AB(\tau)\Gamma(\tau+2)} \sum_{q=2}^{n} \frac{1}{\Delta t} \left[ t_{q-1}^{1-\xi}\, \mathscr{D}_S(t_{q-1},U_{q-1}) - t_{q-2}^{1-\xi}\, \mathscr{D}_S(t_{q-2},U_{q-2}) \right] \mathscr{A}_2(n,q) \\
&+ \frac{\tau(\Delta t)^\tau}{AB(\tau)\Gamma(\tau+3)} \sum_{q=2}^{n} \frac{1}{\Delta t^2} \left[ t_q^{1-\xi}\, \mathscr{D}_S(t_q,U_q) - 2t_{q-1}^{1-\xi}\, \mathscr{D}_S(t_{q-1},U_{q-1}) + t_{q-2}^{1-\xi}\, \mathscr{D}_S(t_{q-2},U_{q-2}) \right] \mathscr{A}_3(n,q),
\end{aligned}
$$

where the coefficients are

$$
\begin{aligned}
\mathscr{A}_1(n,q) &= (n-q+1)^\tau - (n-q)^\tau, \\
\mathscr{A}_2(n,q) &= (n-q+1)^\tau (n-q+3+2\tau) - (n-q)^\tau (n-q+3+3\tau), \\
\mathscr{A}_3(n,q) &= (n-q+1)^\tau \left[2(n-q)^2 + (3\tau+10)(n-q) + 2\tau^2 + 9\tau + 12\right] \\
&\quad - (n-q)^\tau \left[2(n-q)^2 + (5\tau+10)(n-q) + 6\tau^2 + 18\tau + 12\right].
\end{aligned}
$$

Identical formulas hold for the other compartments $V,E,I,R$ by replacing $\mathscr{D}_S$ with $\mathscr{D}_V, \mathscr{D}_E, \mathscr{D}_I, \mathscr{D}_R$.

The rubella model with the Atangana-Baleanu-Caputo (ABC) derivative of order $\beta$ is

$$
\begin{aligned}
{}_0^{ABC}D_t^\beta S &= \Lambda - (\beta I + \mu + \phi)S, \\
{}_0^{ABC}D_t^\beta V &= \phi S - (\beta_v I + \mu)V, \\
{}_0^{ABC}D_t^\beta E &= (\beta S + \beta_v V)I - (\alpha + \mu)E, \\
{}_0^{ABC}D_t^\beta I &= \alpha E - (\gamma + \mu + \delta)I, \\
{}_0^{ABC}D_t^\beta R &= \gamma I - \mu R.
\end{aligned}
$$

Using the same Newton polynomial approach (two-step Lagrange interpolation) we obtain the discrete scheme for $S$:

$$
\begin{aligned}
S_{n+1} &= S(0) + \frac{1-\beta}{ABC(\beta)}\left[\Lambda - (\beta I_n + \mu + \phi)S_n\right] \\
&+ \frac{\beta}{ABC(\beta)}\sum_{j=0}^{n}\left[\frac{h^\beta}{\Gamma(\beta+2)}\Big((n-j+1)^\beta(n-j+2+\beta) - (n-j)^\beta(n-j+2+2\beta)\Big)\right. \\
&\times \big(\Lambda - (\beta I_j + \mu + \phi)S_j\big) - \frac{h^\beta}{\Gamma(\beta+2)}\Big((n-j+1)^{\beta+1} - (n-j)^\beta(n-j+1+\beta)\Big) \\
&\left.\times \big(\Lambda - (\beta I_{j-1} + \mu + \phi)S_{j-1}\big)\right].
\end{aligned}
$$

Analogous expressions hold for the other compartments. Here $h$ is the time step, $t_n = nh$, and $ABC(\beta) = 1 - \beta + \frac{\beta}{\Gamma(\beta)}$ is the normalisation function.

## 5. Numerical simulation

By focusing upon the influence of fractional derivatives on the dynamics of disease, the non- linear epidemic model of the Rubella disease is analyzed in this part. With the aim of gaining the numerical solutions, ABC and FFM operators are utilized which show as a deep understanding that by varying the fractional order also varies the behaviour of the system. The initial conditions are given S(0) = 20,E(0) = 10,I(0) = 8,R(0) = 5,V(0) = 3. and parameters values are listed in Table 1. The ABC derivative introduces memory effects into each compartment: The fractional order controls how quickly changes in infection rates affect susceptibility. For fractional order less than 1, the compartment exhibits memory, meaning past exposure history influences current susceptibility levels. Vaccination effects persist longer under fractional dynamics. The Mittag-Leffler kernel allows for power-law decay of vaccine protection rather than exponential decay. The latent period distribution becomes heavy-tailed, capturing the heterogeneity in incubation periods across individuals. The infectious period follows a stretched exponential distribution, better representing real rubella infectiousness profiles. Lifelong immunity is maintained through the memory effect, but waning immunity would follow a power-law pattern.

The fractal-fractional operator adds an additional fractal dimension that captures the self-similar nature of disease spread: Fractal dimension represents the heterogeneity of the contact network. Fractal dimension one corresponds to classical mixing, while less than one indicates sub-diffusion and greater than 1 indicates super-diffusion. The fractal derivative of susceptible humans modulates the rate at which individuals become exposed. Lower fractal dimension slows down the initial spread, mimicking spatially clustered populations. The fractal dimension affects how quickly vaccination campaigns reach susceptible individuals. For fractal dimension less than 1, vaccination campaigns have prolonged but less intense effects. The exposed and infected humans are most sensitive to fractal dimension because transmission depends on contact patterns. Super-diffusive spread leads to faster outbreaks with higher peaks, while sub-diffusive spread leads to flatter, prolonged epidemics. The fractal dimension affects the accumulation of immunity in the population, with fractal dimension less than 1 leading to slower saturation.

For short-term dynamics, under ABC operator, initial growth is slower than integer-order due to memory. The peak time is delayed, and the peak magnitude is reduced. For FFM operator, initial growth depends strongly on fractal dimension. For fractal dimension smaller than 1, growth is even slower than ABC, while for fractal dimension greater than 1, growth can be faster than integer-order. For medium-term dynamics, under ABC operator, oscillations are damped, and the system converges to endemic equilibrium faster than integer-order. For FFM operator, the fractal dimension can induce sustained oscillations or chaos. For certain fractal values, the system may never settle to equilibrium. For long-term dynamics, under ABC operator, steady-state values are similar to integer-order but reached via a different transient path. Under FFM operator, steady-state may differ significantly from integer-order, especially when fractal dimension is away from 1. The susceptible humans decay initially due to vaccination, transmission and natural death rate but this decay under ABC operator is slower than integer-order operator, while the decay under FFM depends on fractal dimension. If fractal dimension is less than 1, initial decay is faster than ABC. If fractal dimension is greater than 1, initial decay is slower than ABC. The shape of the susceptible curve decay exponentially under ABC operator, while for FFM operator, the

curve depends on fractal dimension. The susceptible humans time to reach 50 % of initial is delayed as compared to integer order, while for FFM operator, time is earlier than ABC operator if fractal dimension is less than 1 and later than ABC operator, if fractal dimension is greater than 1. Memory slows down susceptibility loss., while fractal scaling changes the rate at which people become exposed based on contact network heterogeneity.

The vaccinated humans grow initially. This growth is smooth under ABC operator. For FFM operator, for fractal dimension less than 1, vaccinated humans quickly increase initially, while for fractal dimension greater than 1, slower initial increase. Under ABC operator, the vaccinated humans increase first and then decline to approach equilibrium position. Under FFM operator, vaccinated humans may exhibit multiple oscillations if fractal dimension is far from 1. Vaccine waning effect under ABC operator follows power-law via Mittag-Leffler. For fractal dimension less than 1, waning appears faster initially but slower later. Memory mimics slow decay of vaccine protection. Fractal scaling captures heterogeneous vaccine coverage across different population subgroups. The peak height of exposed humans is lower than integer order operator. The exposed humans under FFM operator are highly sensitive to fractal dimension. Fractal dimension less than 1 gives higher peak. Fractal dimension greater than 1 gives lower peak. The exposed humans experience delay behaviour as compared to integer-order. For FFM operator, exposed humans are earlier than ABC if fractal dimension is less than 1 and later than ABC if fractal dimension is greater than 1. Duration of exposed pool is longer due to memory. For FFM operator, tail behavior is controlled by both fractional order and fractal dimension. Memory captures variation in rubella incubation period. Fractal scaling captures age-structured exposure patterns. The peak infectious under ABC operator is lower than integer-order. Under FFM operator, peak infectious can be higher or lower than ABC. Fractal dimension is less than 1 gives peak infectious higher than ABC, while fractal dimension larger than 1 gives peak infectious lower than ABC. Peak time under ABC are delayed by weeks to months. Under FFM operator, for small fractal dimension, peak occurs earlier than ABC. For fractal dimension greater than 1, peak occurs later than ABC. Epidemic duration under ABC operator is longer than integer-order. For fractal dimension smaller than 1, epidemic duration is even longer than ABC. For fractal dimension greater than 1, epidemic duration is shorter than ABC. Under ABC operator, oscillations after peak are damped and system reaches endemic equilibrium. Under FFM operator, may exhibit sustained oscillations for certain fractal dimensions. Under ABC operator, Second outbreak is unlikely unless new susceptible enter. Under FFM operator, Second outbreak is possible due to fractal scaling. Memory explains why rubella outbreaks have long tails. Fractal scaling explains why rubella outbreaks vary dramatically between rural and urban settings. For recovered humans, saturation rate is slower than integer-order under ABC operator. Memory delays accumulation of immunity. For fractal dimension less than 1, faster initial saturation. For fractal dimension greater than 1, slower initial saturation occurs under FFM operator. The recovered humans exhibit symmetric S-shaped curve. Under FFM operator, fractal dimension less than 1 gives rapid rise, while fractal dimension greater than 1 gives slow rise then rapid.

This difference is due to the reason that ABC only captures temporal memory. Some people develop symptoms in 12 days, others in 21 days. ABC spreads this out. Protection doesn't disappear suddenly but fades slowly. ABC models this. FFM adds spatial/fractal heterogeneity. Rubella spreads differently in schools (fractal dimension greater than 1, super-diffusion) vs. households (fractal dimension greater than 1, sub-diffusion). Vaccination campaigns reach urban areas faster than rural areas, fractal scaling captures this delay. Some communities become immune early, others remain susceptible, FFM allows this clustering.

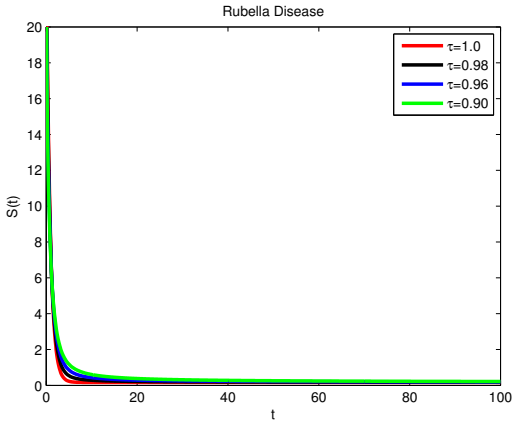


**(a)** Behaviour of susceptible humans under fractal fractional operator with dimension 1.

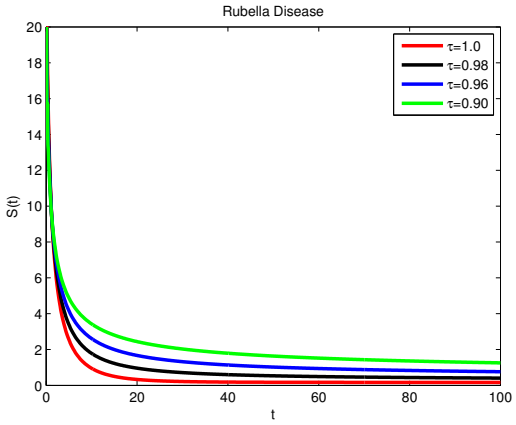


**(b)** Behaviour of susceptible humans under fractal fractional operator with dimension 0.5.

**Figure 6:** Solutions of susceptible humans under FFM operator at different fractional orders.

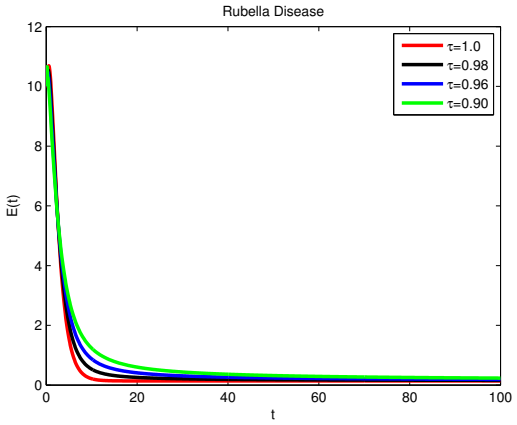


**(a)** Behaviour of exposed humans under fractal fractional operator with dimension 1.

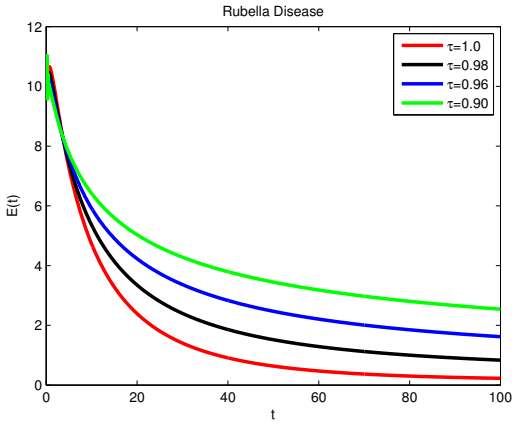


**(b)** Behaviour of exposed humans under fractal fractional operator with dimension 0.5

**Figure 7:** Solutions of exposed humans under FFM operator at different fractional orders.

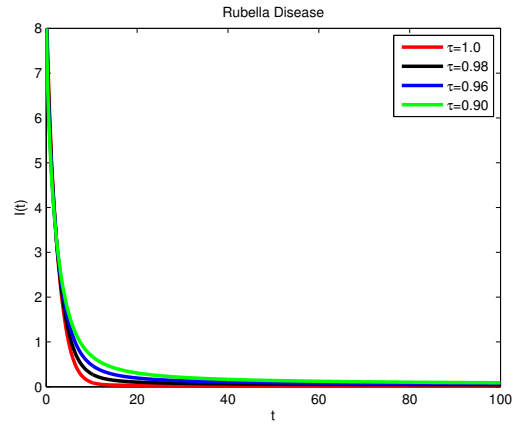


**(a)** Behaviour of infected humans under fractal fractional operator with dimension 1.

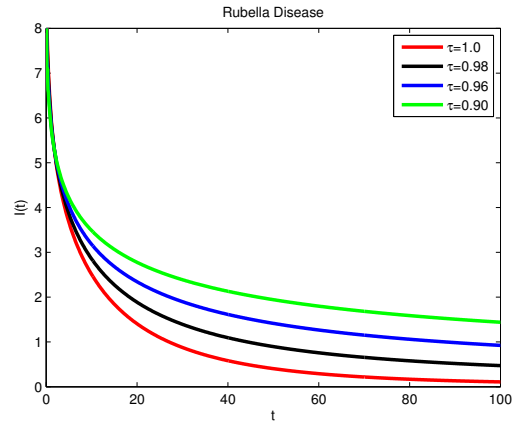


**(b)** Behaviour of infected humans under fractal fractional operator with dimension 0.5

**Figure 8:** Solutions of infected humans under FFM operator at different fractional orders.

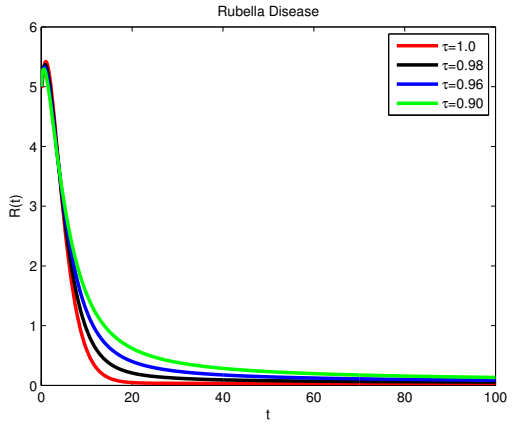


**(a)** Behaviour of recovered humans under fractal fractional operator with dimension 1.

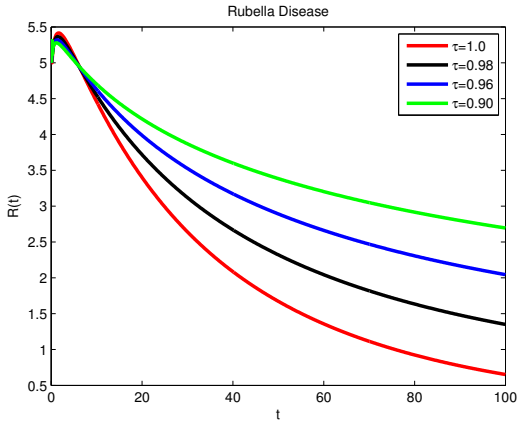


**(b)** Behaviour of recovered humans under fractal fractional operator with dimension 0.5.

**Figure 9:** Solutions of recovered humans under FFM operator at different fractional orders.

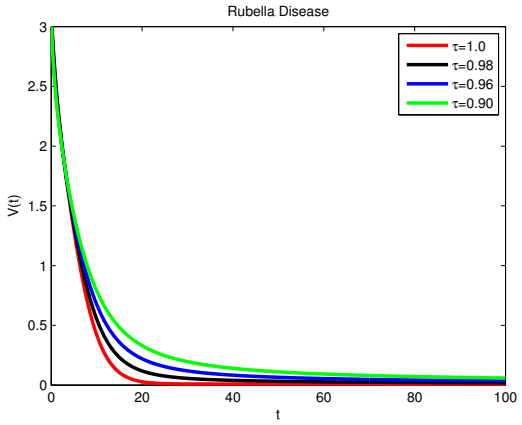


**(a)** Behaviour of vaccinated humans under fractal fractional operator with dimension 1.

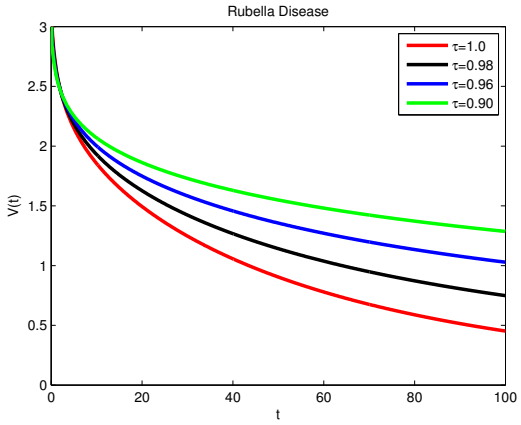


**(b)** Behaviour of vaccinated humans under fractal fractional operator with dimension 0.5.

**Figure 10:** Solutions of vaccinated humans under FFM operator at different fractional orders.

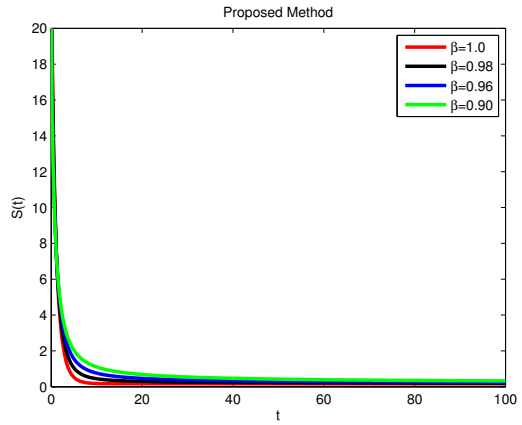


**(a)** Behaviour of susceptible humans under ABC operator with dimension 1

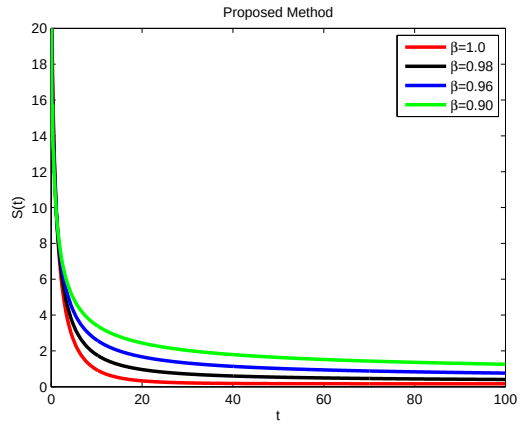


**(b)** Behaviour of susceptible humans under ABC operator with dimension 0.5

**Figure 11:** Solutions of susceptible humans under ABC operator at different fractional orders.

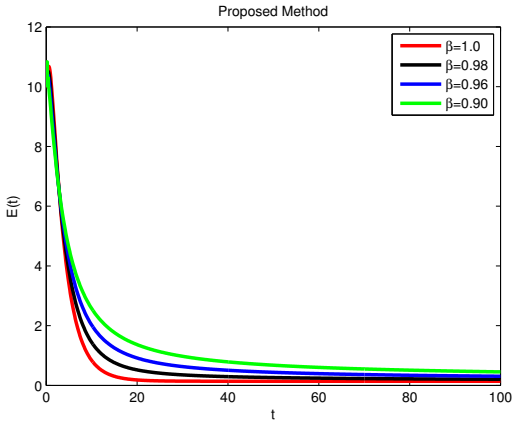


**(a)** Behaviour of exposed humans under ABC operator with dimension 1

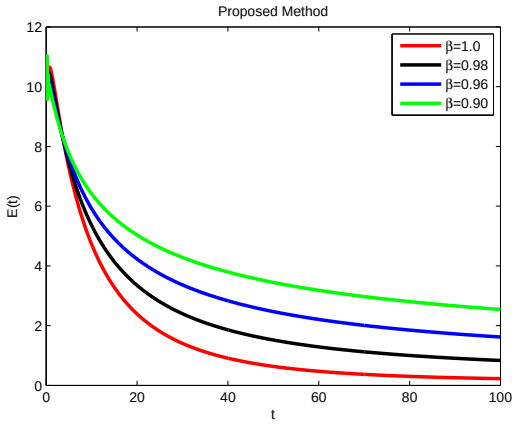


**(b)** Behaviour of exposed humans under ABC operator with dimension 0.5

**Figure 12:** Solutions of exposed humans under ABC operator at different fractional orders.

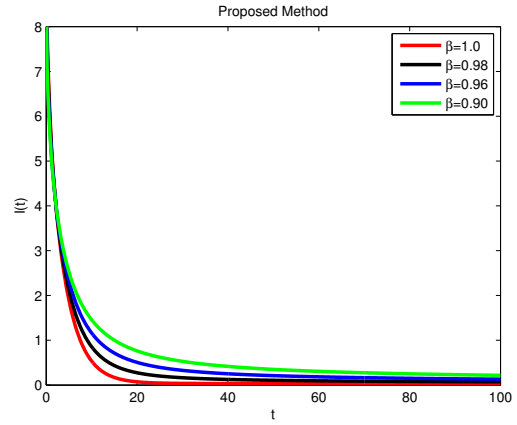


**(a)** Behaviour of infected humans under ABC operator with dimension 1.

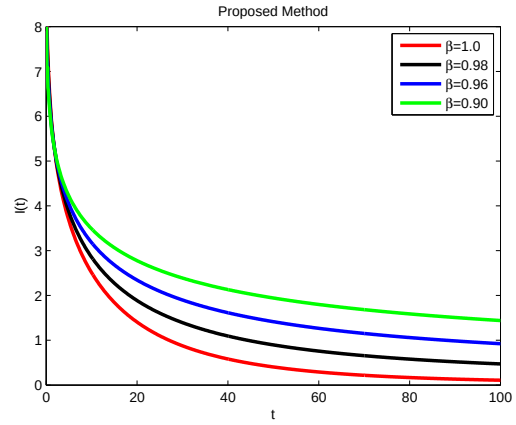


**(b)** Behaviour of infected humans under ABC operator with dimension 0.5

**Figure 13:** Solutions of infected humans under ABC operator at different fractional orders.

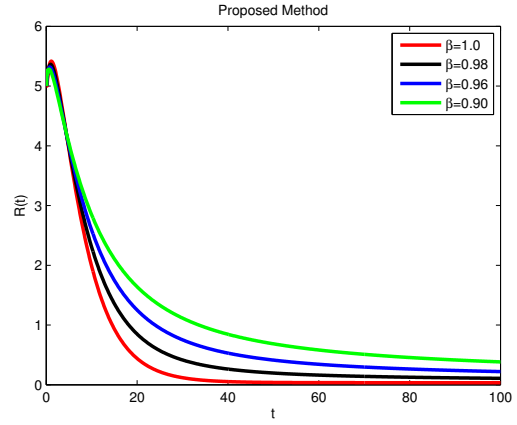


**(a)** Recovered humans under ABC operator wit dimension 1

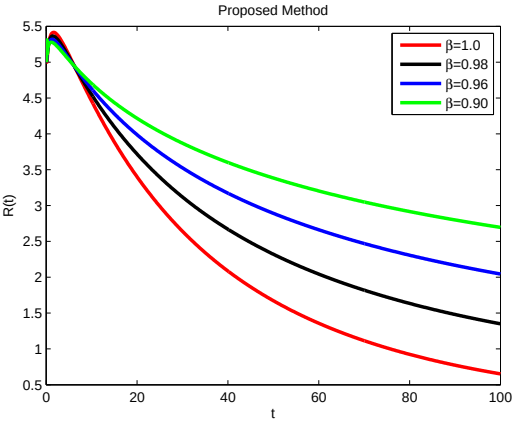


**(b)** Recovered humans under ABC operator with dimension 0.5

**Figure 14:** Solutions of recovered humans under ABC operator at different fractional orders.

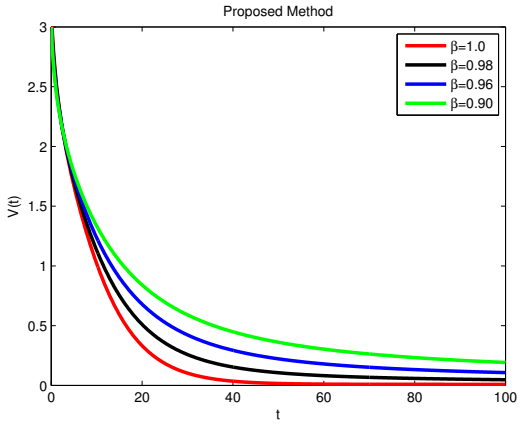


**(a)** Behaviour of vaccinated humans under ABC operator with dimension 1

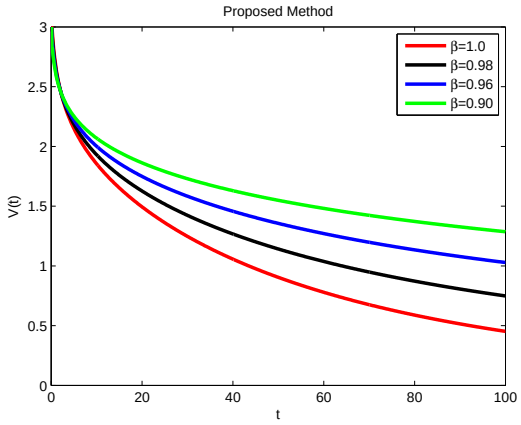


**(b)** Behaviour of vaccinated humans under ABC operator with dimension 0.5

**Figure 15:** Solutions of vaccinated humans under ABC operator at different fractional orders.

## 6. Conclusion

In this study, we have applied the FFM and ABC operators under different fractional orders and fractal dimensions to examine the Rubella model's dynamics offering a deeper understanding of its spread and control under various mathematical conditions. We have verified the presence of a single, positive and bounded solution, providing a mathematical foundation. We have derived the equilibrium points, computed the reproduction number $R_0$ and verified the local and global stability of the equilibrium points. We also have proved the existence of a transcritical bifurcation at $R_0 = 1$ using center manifold theory. This analysis provides a rigorous mathematical foundation for rubella elimination strategies, showing that vaccination coverage sufficient to maintain $R_0 < 1$ is necessary and sufficient for disease eradication. The impact of parameters on compartments shows that sustained vaccination coverage of at least 95% for a minimum of one dose of a rubella-containing vaccine at all levels is recommended to achieve elimination. The chaos 0-1 test shows that model experiences bounded behaviour. The statistical analysis for all compartments has verified the bounded behaviour of all compartments. To approximate the solution, the Newton polynomial based numerical scheme has been constructed. We also have provided comparison of solutions under both operators to verify the reliability of the solution. The analysis confirms that rubella elimination requires $R_0 < 1$, achievable through vaccination coverage exceeding $1 - 1/R_0$. The ABC and FFM fractional operators provide powerful mathematical frameworks for modeling rubella transmission dynamics. The ABC operator captures memory effects through the Mittag-Leffler kernel, while the FFM operator additionally accounts for fractal scaling in contact networks. Both operators represent significant improvements over classical integer-order models and provide more accurate representations of real rubella outbreak patterns.

The sensitivity analysis shows that infectious compartment is the most sensitive to parameter variations. Also the transmission rate $\beta$ is the most influential parameter, strongly affecting S, E, and I compartments, while having only indirect effects on V and R. The analysis communicates that vaccination primarily affects S and V, while recovery primarily affects I and R, and progression primarily affects E. So the most effective way to reduce peak infectious cases is to simultaneously increase vaccination coverage and improve case management. The vaccination campaigns should target populations with high recruitment rates to maintain high V levels over time. The latent period of rubella provides a natural window for contact tracing and quarantine before individuals become infectious. The sensitivity analysis confirms that transmission control ($\beta$ reduction via hygiene, masks, distancing) and vaccination are the two most impact-ful interventions for rubella elimination.

The model assumes homogeneous mixing, which may oversimplify real-world contact patterns. Parameter values are taken from literature and may not capture local epidemiological heterogeneity. The fractional and fractal-fractional operators introduce additional complexity, and their biological interpretation remains partially exploratory. Data on rubella incidence are often under-reported, especially in low-income regions, which could affect model validation. In future, one can incorporate age-structured compartments to better capture rubella dynamics in children and pregnant women. Use spatially explicit models to account for regional differences in vaccination coverage. Apply the fractional framework to other vaccine-preventable diseases (e.g., measles, mumps) for comparative studies. Develop real-time forecasting tools using the FFM formulation combined with

machine learning for outbreak prediction. Explore optimal control strategies (e.g., time-dependent vaccination) under fractional dynamics.

### Conflict of Interest

The authors declare that there is no conflict of interest regarding the publication of this manuscript.

### Data Availability:

The data used in this study are available upon reasonable request.

### Authors' Contributions :

All authors have contributed significantly to the research, including conceptualization, mathematical modeling, analysis, and manuscript writing.

### References


[1] Rubella. In *Wikipedia*. Retrieved June 14, 2026, from https://en.wikipedia.org/wiki/Rubella

[2] World Health Organization (WHO). *Rubella – number of reported cases*. Global Health Observatory data. Retrieved June 14, 2026, from https://www.who.int/data/gho/data/indicators/indicator-details/GHO/rubella---number-of-reported-cases

[3] Hasnan, N. H., & Puzi, S. M. Numerical Solution for Rubella Transmission With Vaccination Effect Using Adaptive Runge-Kutta Method.

[4] Ochigbo, J. E., Okorie, C. E., & Ojeka, P. I. Dynamics of Measles-Rubella co-circulation: A mathematical model incorporating waning immunity, isolation, vertical transmission and adaptive public health response.

[5] Zeb, S., Yatim, S. A. M., Ahmad, A., Kamran, A., & Rafiq, M. (2025). Numerical modelling of SEIR on two-dose vaccination against the rubella virus. *Malaysian Journal of Fundamental and Applied Sciences*, 21(1), 1577-1601.

[6] Zhang, Y., Zhang, T., & Li, Z. (2025). A RUBELLA EPIDEMIC MODEL WITH SEASONALITY. *Journal of Applied Analysis & Computation*, 16(3), 1207-1225.

[7] Tilahun, G. T., Tolasa, T. M., & Wole, G. A. (2022). Modeling the dynamics of rubella disease with vertical transmission. *Heliyon*, 8(11).

[8] Peter, O. J., Kumari, N., Kumar, A., Omede, B. I., Ogunmola, O. P., Balogun, G. B., & Godara, G. (2026). Analysis and dynamics of rubella with control strategies: a data-driven mathematical modeling approach. *Boletín de la Sociedad Matemática Mexicana*, 32(1), 36.

[9] Amelia, D., & Tasman, H. (2021, January). Mathematics model of measles and rubella with vaccination. *Journal of Physics: Conference Series (Vol. 1725, No. 1, p. 012017). IOP Publishing*.

[10] Jain, K., & Bhattacharjee, A. (2022). Mathematical Modeling of Rubella Disease Dynamics with Vertical Transmission. *Globl Journal of Pure and Applied Mathematics*, 18, 392-400.

[11] Tilahun, G. T., Tolasa, T. M., Asfaw, M. D., & Wole, G. A. (2024). Stochastic and deterministic models for Rubella dynamics with two doses of vaccination and vertical transmission. *Discrete Dynamics in Nature and Society*, 2024(1), 9697951.

[12] Ahmad, W., Butt, A. I. K., Akhtar, N., Rafiq, M., Gohar, M., Idrees, Z., & Ahmad, N. (2024). Developing computationally efficient optimal control strategies to eradicate Rubella disease. *Physica Scripta*, 99(3), 035202.

[13] Duru, E. C., Anyanwu, M. C., & Nwosu, C. N. (2023). Optimal vaccination and treatment strategies for control of rubella with vertical transmission. *International Journal of Mathematical Analysis and Modelling*, 6(2).

[14] Asri, M., Sidjara, S., Sanusi, W., Side, S., & Pratama, M. I. (2021, May). Analysis and solution of the SEIRS model for the Rubella transmission with vaccination effect using Runge-Kutta method. *Journal of Physics: Conference Series (Vol. 1899, No. 1, p. 012090). IOP Publishing*.

[15] Prawoto, B. P., Abadi, & Artiono, R. (2020, September). Dynamic of re-infection Rubella transmission model with vaccination. *AIP conference Proceedings (Vol. 2264, No. 1, p. 020005). AIP Publishing LLC*.

[16] Younus, A., Asif, M., Atta, U., Bashir, T., & Abdeljawad, T. (2023). Applications of fuzzy conformable Laplace transforms for solving fuzzy conformable differential equations. *Soft Computing*, 27(13), 8583-8597.

[17] Abdeljawad, T., Younus, A., Alqudah, M., & Atta, U. (2023). On fuzzy conformable double laplace transform with applications to partial differential equations. *Computer Modeling in Engineering & Sciences*, 134(3), 2163.

[18] Caputo, M., and Fabrizio, M. (2015). A new definition of fractional derivative without singular kernel. *Progress in Fractional Differentiation & Applications*, 1(2), 73-85.

[19] Losada, J., & Nieto, J. J. (2015). Properties of a new fractional derivative without singular kernel. *Progr. Fract. Differ. Appl*, 1(2), 87-92.

[20] Atangana, A., & Baleanu, D. (2016). New fractional derivatives with nonlocal and non-singular kernel: theory and application to heat transfer model. *arXiv preprint arXiv*:1602.03408.

[21] Atangana, A. (2017). Fractal-fractional differentiation and integration: connecting fractal calculus and fractional calculus to predict complex system. *Chaos, solitons and fractals*, 102, 396-406.

[22] Ahmad, W., Nazir, M. A., Rafiq, M., Butt, A. I. K., Ahmad, N., & Hussain, M. (2025). Analyzing optimal control techniques in a nonlinear fractional Rubella model with the Atangana–Baleanu derivative. *Computers in Biology and Medicine*, 197, 110954.

[23] Elivina, E. F., & Kusumawinahyu, W. M. (2023). Dynamics of a fractional-order rubella disease model with vertical transmission and saturated incidence rate. *Communications in Mathematical and Biological Neurosciences*, 2023, Article-ID.

[24] Atangana, A., & Alkahtani, B. S. T. (2016). Modeling the spread of R ubella disease using the concept of with local derivative with fractional parameter: Beta-Derivative. *Complexity*, 21(6), 442-451.

[25] Al Qurashi, M. M. (2020). Role of fractal-fractional operators in modeling of rubella epidemic with optimized orders. *Open Physics*, 18(1), 1111-1120.

[26] Koca, I. (2018). Analysis of rubella disease model with non-local and non-singular fractional derivatives. *An International Journal of Optimization and Control*, 8(1), 17-25.

[27] Alkahtani, B. S. T. (2023). Dynamical analysis of Rubella disease model in the context of fractional piecewise derivative: simulations with real statistical data. *Fractal and Fractional*, 7(10), 746.

[28] Owolabi, K. M., Gómez-Aguilar, J. F., & Karaagac, B. (2019). Modelling, analysis and simulations of some chaotic systems using derivative with Mittag–Leffler kernel. *Chaos, Solitons & Fractals*, 125, 54-63.

[29] Farman, M., Ahmad, A., Atta, U., Nisar, K. S., & Ghaffar, A. (2025). Hyers Ulam stability and bifurcation control of leptospirosis disease dynamics and preventations: Modeling with singular and non-singular kernels.*PloS one*, 20(3), e0314095.

[30] Shah, K., Arfan, M., Mahariq, I., Ahmadian, A., Salahshour, S., and Ferrara, M. (2020). Fractal-fractional mathematical model addressing the situation of corona virus in Pakistan. *Results in physics, 19*, 103560.

[31] Diekmann, O., Heesterbeek, J. A. P., & Roberts, M. G. (2010). The construction of next-generation matrices for compartmental epidemic models. *Journal of the royal society interface*, 7(47), 873-885.

[32] Castillo-Chavez, C. (2002). On the computation of R. and its role on global stability Carlos Castillo-Chavez*, Zhilan Feng, and Wenzhang Huang. *Mathematical approaches for emerging and reemerging infectious diseases: an introduction*, 1, 229.

[33] Gottwald, G. A., & Melbourne, I. (2004). A new test for chaos in deterministic systems. Proceedings of the Royal Society of London. Series A: Mathematical, Physical and Engineering Sciences, 460(2042), 603-611.

[34] Gottwald, G. A., & Melbourne, I. (2009). On the implementation of the 0–1 test for chaos. SIAM Journal on Applied Dynamical Systems, 8(1), 129-145.

[35] Ahmad, A., Atta, U., Akgül, A., Sattar, S., & Ahmad, M. O. (2025). A study on mathematical modeling and control of leptospirosis transmission dynamics during a hurricane with asymptomatic measures.*Modeling Earth Systems and Environment*, 11(5), 361.

[36] Atangana, A., & Araz, S. I. (2021). New numerical scheme with Newton polynomial: theory, methods, and applications. *Academic Press*.